

# Virtual sources and receivers in the real Earth, a method for induced seismicity monitoring

Joeri Brackenhoff<sup>1,2</sup>, Jan Thorbecke<sup>1</sup>, and Kees Wapenaar<sup>1</sup>

<sup>1</sup>Department of Geoscience and Engineering, Delft University of Technology,  
Stevinweg 1, 2628 CN Delft, The Netherlands

<sup>2</sup>J.A.Brackenhoff@tudelft.nl

April 8, 2022

## **Abstract**

To enhance the monitoring of the subsurface, virtual receivers can be deployed, which can be created by the Marchenko method. These virtual receivers are used to study real source signals in the subsurface. To use the virtual receivers with a real source, homogeneous Green's function retrieval is required. Classical homogeneous Green's function retrieval requires an enclosing recording surface, however by using a single-sided retrieval scheme, this requirement can be avoided. We first show that the construction of a homogeneous Green's function on a field dataset from the Vøring basin can be achieved. To this end, we show the retrieval of virtual receivers on a synthetic dataset that is based on the field dataset. Because the Marchenko method is sensitive to recording limitations with the reflection data, we consider several limitations on the synthetic data. We take these limitations into account for the field dataset, by processing the reflection data. A comparison is made between the single-sided and classical retrieval of the homogeneous Green's function. We consider two different mechanisms for the virtual source, a monopole point source and a double-couple source. The homogeneous Green's function retrieved from the field data shows potential for monitoring of the wavefield and the source mechanism.

# 1 Introduction

One of the primary reasons seismic reflection methods are used is to explore the subsurface in a non-invasive way. In seismic exploration, active seismic sources and receivers, placed at the surface of the Earth, are usually employed for the purpose of imaging and monitoring. This results in reflection data of the subsurface and includes the primary and multiple scattering of wavefields in the subsurface. Responses to passive sources can be measured as well, for example in the case of induced seismicity. Induced seismicity has been an important topic in countries such as the United States (Magnani et al., 2017) and the Netherlands (van Thienen-Visser and Breunese, 2015), where its effects on the surrounding area are the subject of much debate. Seismic measurements can be used to help determine the source location and mechanism of these earthquakes and time-lapse measurements can help to determine the changes in geomechanical properties of the area. Ideally, seismic measurements should be done with receivers inside the medium, for example by using borehole receivers, however this is an unpractical and expensive process, particularly for deep boreholes.

An alternative approach to physically placing the receivers in the subsurface is the use of virtual receivers. A virtual receiver is created by using advanced processing techniques to relocate the wavefield response from the physical receivers at the surface of the medium to any location inside the medium, accounting for multiple reflections. This can be achieved by the use of the Marchenko method, which has been developed in the last few years. It was first proposed for 1D methods (Broggini et al., 2012) based on work for autofocusing by Rose (2001) and further extended for 2D and 3D applications (Wapenaar et al., 2014). The method uses single-sided reflection data at the surface and an estimation of the first arrival between the surface and the desired virtual receiver location. This first arrival can be estimated from a smooth background velocity model. The Marchenko method is data-driven, which means that no detailed model is required to redatum the virtual receiver location. If virtual receiver locations are created for many different locations in the subsurface, it can replace the need for the physical receivers. In this application of the Marchenko method, the source will still be located at the surface of the Earth, however.

In the case of induced seismicity, there will be a passive recording at the surface of the medium, which gives opportunity for monitoring. To monitor the induced seismicity source in the medium using virtual receivers, an additional step needs to be taken, called homogeneous Green's function retrieval. A Green's function is the wavefield response of the medium to a Dirac delta source. The homogeneous Green's function is a Green's function superposed with its time-reversal, which avoids a singularity at the source location. Porter (1970) derived a representation which entails that if two Green's functions with sources inside the medium are recorded on a boundary enclosing the medium, the homogeneous Green's function between the two source locations can be retrieved. This classical representation was further extended for inverse source problems by Porter and Devaney (1982) and for inverse scattering methods by Oristaglio (1989). The method could in principle be used to combine the induced seismicity recording at the surface with a virtual receiver inside the medium to retrieve the response at the virtual receiver location to the induced seismicity source. However, for the classical representation it appeared that the requirement of an enclosing recording surface is vital if one wants to avoid artifacts related to erroneously handles scattering in the final result.

In recent years a new representation for homogeneous Green's function retrieval has been derived, related to the Marchenko method. Instead of an enclosing boundary it uses a single boundary (Wapenaar et al., 2017). An example of the application of this method on synthetic data can be found in Wapenaar et al. (2016). Applying the method on field data is challenging, due to practical limitations of the Marchenko method. In the derivation of the Marchenko method, evanescent waves are ignored and it is assumed that the medium is lossless, which is

invalid in real media. Furthermore, the reflection response needs to be well sampled and the aperture needs to be sufficiently large. In the past few years the method has been successfully applied on field data for the purpose of imaging. Examples can be found in Ravasi et al. (2016) and Staring et al. (2018), who used adaptive corrections to the data to successfully apply the Marchenko method.

The aim of this work is to apply the Marchenko method on a field dataset from the Vøring basin to create virtual receivers, which are used to monitor a source signal in the subsurface. The monitored source can be real or virtual. In our application, because there is no induced seismicity recording available in the area of interest, the Marchenko method is used to create a virtual source in the subsurface, through the use of source-receiver reciprocity. To determine the need for adaptive corrections, we first consider common issues with the recording of the reflection response and their effect on the final result in greater detail. This is done by building a model based on images retrieved from the field dataset. The modeled data are truncated to mimic the field data more closely, and to demonstrate the effects of practical limitations on the retrieval of the homogeneous Green's function. To ensure these effects are avoided on the field data, adaptive corrections to the field reflection response are applied before it is used in the single-sided representation. We compare the result and show that the method can be applied successfully on field data and can be used to monitor induced seismicity using the same principle.

## 2 Theory

In this section, we present an overview of the definitions and equations that are required for homogeneous Green's function retrieval. The Green's function and focusing function are reviewed, followed by the definitions of the classical and single-sided retrieval schemes for the homogeneous Green's function. The Marchenko method and its limitations are also considered.

### 2.1 Green's function

The Green's function is defined as the solution of the medium that obeys the acoustic wave equation with a unit point source:

$$\left( \rho(\mathbf{x}) \partial_i \left( \frac{1}{\rho(\mathbf{x})} \partial_i \right) - \frac{1}{c^2(\mathbf{x})} \partial_t^2 \right) G(\mathbf{x}, \mathbf{x}_S, t) = -\rho(\mathbf{x}) \delta(\mathbf{x} - \mathbf{x}_S) \partial_t \delta(t), \quad (1)$$

or in the frequency domain:

$$\left( \rho(\mathbf{x}) \partial_i \left( \frac{1}{\rho(\mathbf{x})} \partial_i \right) + \frac{\omega^2}{c^2(\mathbf{x})} \right) G(\mathbf{x}, \mathbf{x}_S, \omega) = -j\omega \rho(\mathbf{x}) \delta(\mathbf{x} - \mathbf{x}_S), \quad (2)$$

where  $G(\mathbf{x}, \mathbf{x}_S, t)$  describes the response of the medium, at time  $t$ , at location  $\mathbf{x}$  to a source at location  $\mathbf{x}_S$ . The locations are defined in 3D such that  $\mathbf{x} = (x_1, x_2, x_3)^T$ . The symbols  $\rho$  and  $c$  indicate the density and velocity of the medium, respectively,  $\delta$  indicates a Dirac delta function,  $\partial_t$  a temporal derivative and  $\partial_i$  the partial derivative in the three principal directions. The subscript follows the Einstein summation convention such that  $\partial_i = (\partial_1, \partial_2, \partial_3)^T$  and  $\partial_i \partial_i = \partial_1^2 + \partial_2^2 + \partial_3^2$ . Note that the source at the right hand side is defined with a temporal derivative acting on the Dirac delta function. This choice is made to simulate a volume injection-rate source, which is closer to reality for seismic surveys. We also consider

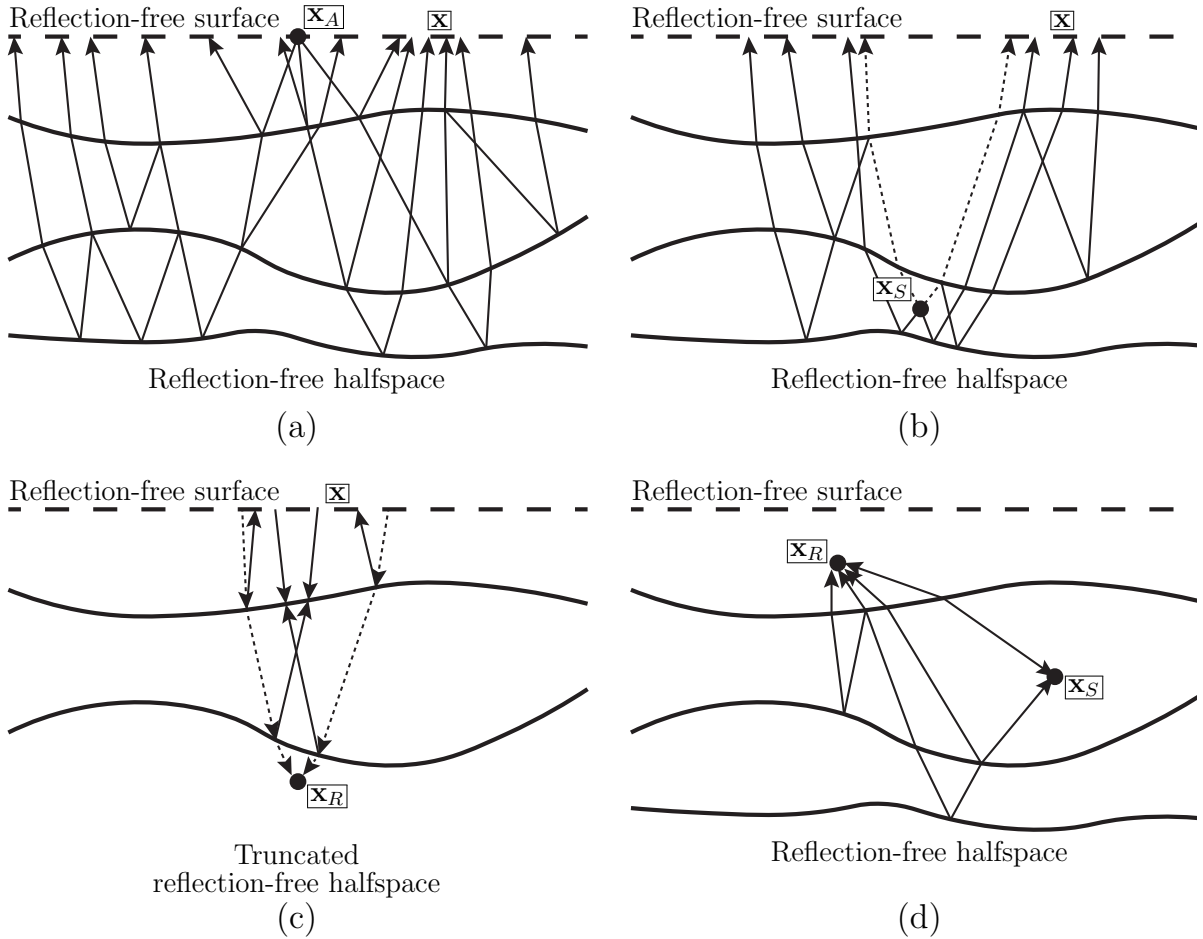


Figure 1: Possible raypaths drawn for, (a) a reflection response  $R(\mathbf{x}, \mathbf{x}_A, t)$ , measured at varying receiver locations  $\mathbf{x}$  at the surface, to a source at  $\mathbf{x}_A$  also at the surface, (b) a Green's function  $G(\mathbf{x}, \mathbf{x}_S, t)$ , measured at varying receiver location  $\mathbf{x}$  at the surface to a source at  $\mathbf{x}_S$  inside the medium, (c) a focusing function  $F(\mathbf{x}_R, \mathbf{x}, t)$ , that is focusing to a focal location  $\mathbf{x}_R$  inside a truncated medium from the surface at varying locations  $\mathbf{x}$ , and (d) a homogeneous Green's function  $G_H(\mathbf{x}_R, \mathbf{x}_S, t)$ , between two locations,  $\mathbf{x}_R$  and  $\mathbf{x}_S$  inside the medium. The dotted lines in (b) and (c) indicate the first arrival for the focusing function and Green's function.

the Fourier transformed Green's function  $G(\mathbf{x}, \mathbf{x}_S, \omega)$  and its complex conjugate  $G^*(\mathbf{x}, \mathbf{x}_S, \omega)$ , which are related to the time domain Green's function by the temporal Fourier transform:

$$G(\mathbf{x}, \mathbf{x}_S, \omega) = \int_{-\infty}^{\infty} G(\mathbf{x}, \mathbf{x}_S, t) \exp(-j\omega t) dt, \quad (3)$$

where  $\omega$  denotes the angular frequency. A schematic illustration of the Green's function is shown in Figure 1-(b), where the receivers are placed on the surface of a medium and its source inside the medium. Figure 1-(a) shows another Green's function, with both its source and receivers placed on the surface of the medium. This is called the reflection response  $R(\mathbf{x}, \mathbf{x}_A, t)$  and contains all the reflections, both primaries and multiples, of the medium, although we assume that the direct wave from the sources to the receivers is not present.

The homogeneous Green's function is defined as the superposition of the Green's function with its time-reversal. Because of the temporal derivative on the Dirac delta function, this results in the right hand source term of equation (1) vanishing, thereby avoiding a source singularity at the source position:

$$G_H(\mathbf{x}, \mathbf{x}_S, t) = G(\mathbf{x}, \mathbf{x}_S, t) + G(\mathbf{x}, \mathbf{x}_S, -t), \quad (4)$$

$$\left( \rho(\mathbf{x}) \partial_i \left( \frac{1}{\rho(\mathbf{x})} \partial_i \right) - \frac{1}{c^2(\mathbf{x})} \partial_t^2 \right) G_H(\mathbf{x}, \mathbf{x}_S, t) = 0, \quad (5)$$

and in the frequency domain:

$$G_H(\mathbf{x}, \mathbf{x}_S, \omega) = G(\mathbf{x}, \mathbf{x}_S, \omega) + G^*(\mathbf{x}, \mathbf{x}_S, \omega), \quad (6)$$

$$\left( \rho(\mathbf{x}) \partial_i \left( \frac{1}{\rho(\mathbf{x})} \partial_i \right) + \frac{\omega^2}{c^2(\mathbf{x})} \right) G_H(\mathbf{x}, \mathbf{x}_S, \omega) = 0, \quad (7)$$

where  $G_H(\mathbf{x}_R, \mathbf{x}_S, t)$  and  $G_H(\mathbf{x}_R, \mathbf{x}_S, \omega)$  denote the homogeneous Green's function in the time domain and frequency domain, respectively. Figure 1-(d) shows a schematic illustration of the homogeneous Green's function, with both its source and receiver inside the medium.

## 2.2 Focusing Function

The focusing function  $F(\mathbf{x}_R, \mathbf{x}, t)$  describes a wavefield, at time  $t$ , at location  $\mathbf{x}$ , that converges to a focal location  $\mathbf{x}_R$  in the subsurface. The focusing function propagates in a truncated medium, which means that there are no reflectors present below the focal location.

The focusing function consists of an up- and downgoing part, which can be combined as follows:

$$F(\mathbf{x}_R, \mathbf{x}, \omega) = f_1^+(\mathbf{x}, \mathbf{x}_R, \omega) - f_1^{-*}(\mathbf{x}, \mathbf{x}_R, \omega), \quad (8)$$

where  $f_1^+(\mathbf{x}_R, \mathbf{x}, \omega)$  denotes the downgoing focusing function and  $f_1^-(\mathbf{x}_R, \mathbf{x}, \omega)$  the upgoing focusing function. The downgoing part of the focusing function is defined as the inverse of the transmission response of the truncated medium.

The focusing function is schematically illustrated in Figure 1-(c). The first arrival, which is indicated by the dotted line, propagates to the focal location and scatters at the reflectors, creating an upgoing wavefield. In order to ensure that these upgoing waves do not cause additional reflections arriving after the focus of the wavefield, downgoing waves are injected, which cancel these reflections. This occurs at the locations of opposite arrows in the figure.

## 2.3 Homogeneous Green's function representation

The classical representation of the homogeneous Green's function states that the response between any two source locations in a medium can be retrieved. In order to achieve this, the response to both these sources must be measured at the exact same locations on a boundary that encloses the medium (Porter, 1970; Porter and Devaney, 1982; Oristaglio, 1989). The classical representation in the frequency domain can be written as follows:

$$G_H(\mathbf{x}_R, \mathbf{x}_S, \omega) = \oint_{\partial \mathbb{D}} \frac{1}{j\omega\rho(\mathbf{x})} \{ \partial_i G^*(\mathbf{x}_R, \mathbf{x}, \omega) G(\mathbf{x}, \mathbf{x}_S, \omega) - G^*(\mathbf{x}_R, \mathbf{x}, \omega) \partial_i G(\mathbf{x}, \mathbf{x}_S, \omega) \} n_i d^2 \mathbf{x}, \quad (9)$$

where  $n_i$  indicates the normal vector in the three principal directions. The integral is evaluated over a boundary  $\partial \mathbb{D}$  enclosing the medium  $\mathbb{D}$ . In equation (9), the function  $G(\mathbf{x}, \mathbf{x}_S, \omega)$  describes the response of the medium at varying location  $\mathbf{x}$  at the boundary to a source at location  $\mathbf{x}_S$  inside the medium. The time-reversed function  $G^*(\mathbf{x}_R, \mathbf{x}, \omega)$  back-propagates the responses from the boundary to the receiver location  $\mathbf{x}_R$ . A schematic representation of this procedure is shown in Figure 2-(a).

In practice, this representation is often not evaluated correctly, because acquisition on an enclosing boundary is not feasible and only measurements on a single-sided boundary are available.

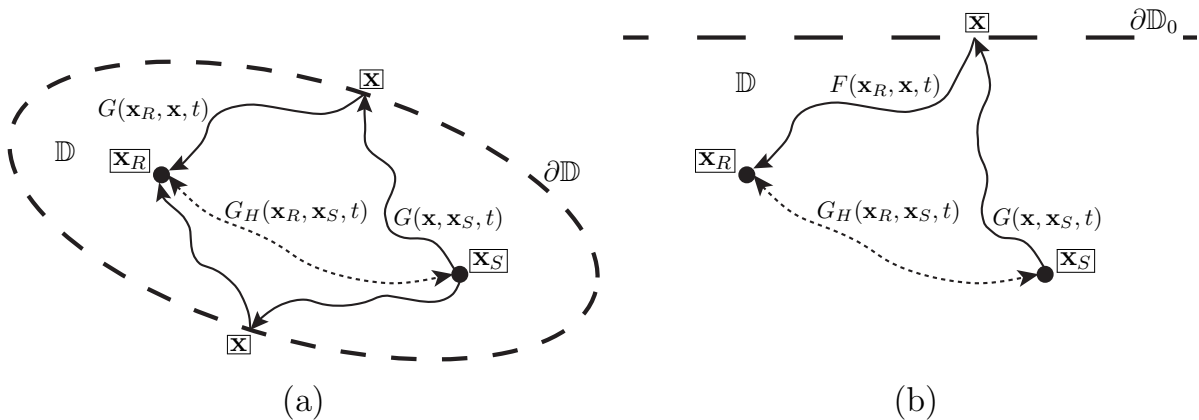


Figure 2: *Recording setup for homogeneous Green's function retrieval using (a) the classical setup and (b) the single-sided setup. For both setups, the same Green's function,  $G(\mathbf{x}, \mathbf{x}_S, t)$  is utilized. For the classical setup an additional Green's function,  $G(\mathbf{x}_R, \mathbf{x}, t)$  is used and the medium  $\mathbb{D}$  is surrounded by an enclosing boundary  $\partial\mathbb{D}$ , over which equation (9) is evaluated. For the single-sided setup the latter Green's function has been replaced by the focusing function,  $F(\mathbf{x}_R, \mathbf{x}, t)$ . The medium  $\mathbb{D}$  is not enclosed and only has a boundary  $\partial\mathbb{D}_0$  at a single side, over which equation (10) is evaluated. In both setups the homogeneous Green's function is indicated by the dotted line.*

As an approximation, equation (9) can be evaluated over the single-sided boundary. Applying the representation in this way causes significant artifacts in the final result. Due to the fact that few alternatives are available, the method is still widely applied to cases where no closed boundaries are present. This approach is equal to injecting the time-reversed Green's function into the medium from the top boundary. If the injection would be performed from all sides, spurious events would cancel due to destructive interference and the wavefield would focus to its original source position. From there, it would act as a source for a wavefield propagating forward in time. However, when the boundary is not enclosing, part of the time-reversed wavefield is missing, hence, the destructive interference does not occur correctly and undesired events will propagate through the medium and cause additional reflections. To limit the artifacts, one of the Green's functions could be replaced by the direct arrival, indicated by the dotted line in Figure 1-(b). As can be seen in this figure, the direct arrival originates at the source location and when it is time-reversed and injected into the medium it will focus back to the source location. During the propagation of the time-reversed direct arrival, reflections will be caused that create artifacts. This approach produces less artifacts, however, it still contains fundamental flaws.

An alternative method that can be used, when the boundary is not closed, is based on the focusing function. This representation is capable of retrieving the homogeneous Green's function from a single-sided boundary, hence it is referred to as the single-sided representation. It can be written as:

$$G_H(\mathbf{x}_R, \mathbf{x}_S, \omega) = \Im \int_{\partial\mathbb{D}_0} \frac{-4}{\omega\rho(\mathbf{x})} \{\partial_3 F(\mathbf{x}_R, \mathbf{x}, \omega) G(\mathbf{x}, \mathbf{x}_S, \omega)\} d^2\mathbf{x}, \quad (10)$$

where  $\partial\mathbb{D}_0$  denotes the single-sided boundary and  $\Im$  the imaginary part of a complex function. In this equation,  $G(\mathbf{x}, \mathbf{x}_S, \omega)$  still functions as the response to the source inside the medium, measured at the single-sided boundary  $\partial\mathbb{D}_0$ . However, in this case, the focusing function  $F(\mathbf{x}_R, \mathbf{x}, \omega)$  serves as the back-propagator of the responses from the boundary to the focal location inside the medium. A schematic representation of this procedure is shown in Figure 2-(b).

The two representations for homogeneous Green’s function retrieval are similar, with the only difference being the focusing function. As one can interpret from Figure 1-(c), the convergence to the focal location is ensured and the coda of the focusing function removes unwanted reflections from the first arrival. The arrival times of the direct wave of the focusing function are the same as the arrival times of the direct wave of the time-reversed Green’s function. The difference is that the coda of the focusing function is designed to cancel out the events that are introduced by using measurements from a single-sided boundary, whereas the coda of the time-reversed Green’s function introduces additional artifacts.

There are two ways that the representations can be employed. The receivers that are used are virtual in both instances, as they are created from the reflection data. The source of the Green’s function  $G(\mathbf{x}, \mathbf{x}_S, \omega)$  on the other hand, can be either a real source or a virtual source. In order to use a real subsurface source, one requires a passive recording at the location of the receiver array in the same medium the reflection data was recorded over. If such a recording is not available, a virtual source can be created. When the medium is reciprocal, it can be obtained by using source-receiver reciprocity on a virtual receiver location. In this paper, both the source and receiver in the subsurface are virtual and no real subsurface source is used.

## 2.4 Marchenko method

We use the Marchenko method to retrieve the focusing function and Green’s function with a virtual receiver inside the medium. A more detailed consideration of the method can be found in the Wapenaar et al. (2014). Here we only consider the equations and properties of the method relevant for this paper. The Green’s function and focusing function inside the medium are related via a reflection response according:

$$G(\mathbf{x}_R, \mathbf{x}_S, t) - F(\mathbf{x}_S, \mathbf{x}_R, -t) = \int_{\partial\mathbb{D}_0} \int_{-\infty}^{\infty} R(\mathbf{x}_R, \mathbf{x}, t') F(\mathbf{x}_S, \mathbf{x}, t - t') dt' d^2\mathbf{x}. \quad (11)$$

Equation (11) states that if the reflection response  $R$  at a boundary  $\partial\mathbb{D}_0$  and a focusing function inside the medium  $\partial\mathbb{D}$  are available, the Green’s function can be retrieved. The retrieval of the focusing function inside the medium can be achieved using the iterative Marchenko equation:

$$F_{k+1}(\mathbf{x}_S, \mathbf{x}_R, -t) = D(\mathbf{x}_S, \mathbf{x}_R, -t) - W(\mathbf{x}_R, \mathbf{x}_S, t) \int_{\partial\mathbb{D}_0} \int_{-\infty}^{\infty} R(\mathbf{x}_R, \mathbf{x}, t') F_k(\mathbf{x}_S, \mathbf{x}, t - t') dt' d^2\mathbf{x}, \quad (12)$$

where  $F_k(\mathbf{x}_S, \mathbf{x}_R, t)$  is the focusing function after  $k$  iterations,  $W(\mathbf{x}_R, \mathbf{x}_S, t)$  is a windowing function that separates the Green’s function and focusing function in time and  $D(\mathbf{x}_S, \mathbf{x}_R, t)$  is the shared first arrival of the focusing function and time-reversed Green’s function. In order to use equation (12) and start the iterative scheme, a first estimation of the focusing function is required. The direct arrival of the time-reversed Green’s function is used as the first estimation. As mentioned before, if this arrival is emitted into the medium, it will cause additional reflections that are not cancelled. By using equation (12), the coda of the focusing function is retrieved, which will suppress the undesired reflections. The only required components for the iterative scheme are a reflection response measured on the single-sided boundary and the direct arrival from the focal point. This direct arrival can be modeled using a smooth velocity model. After the focusing function has been retrieved, it can be used in equation (11) to produce the Green’s function. All the Green’s functions and focusing functions in this paper were retrieved using the Marchenko method to keep the comparison between the modeled data and the field data situation as fair as possible.

The Marchenko method has restrictions when it is applied on field data. An important limitation of the Marchenko method that is considered in this paper is that no free-surface multiples

can be present in the reflection response. There are ways to incorporate these multiples in the method as well, for an example see Singh et al. (2015). Additionally, the reflection response that is used needs to be accurate, as issues with the recording have strong influences on the final result. An important requirement is that the medium in which the reflection response is recorded needs to be lossless (hence, there can be no attenuation). Also, the reflection response needs to, preferably, be densely sampled, contain both positive and negative offsets and have sufficient recording length. If synthetic data are used, the reflection response can be modeled without these limitations. However, when field data are recorded, not all of these requirements can be fulfilled.

### 3 Methods

#### 3.1 Available data

The considered field data were recorded in a marine setting over the Vøring basin by SAGA Petroleum A.S., which is currently part of Equinor. The data consists of a 2D reflection response with a moving spread. The parameters of the recording can be found in table 1. An example of a single common-source record is shown in Figure 3-(a), where the data have been convolved with a 30 Hz Ricker wavelet for display purposes. There are several events present in the common-source record, however it should be noted that the near offsets are missing. This is inherent in the case of marine recordings, because receivers cannot be placed too close to active sources. The sources and receivers are located inside the water, and because S-waves cannot propagate in water, only P-waves are measured by the receivers. There are conversions from P-waves to S-waves and back in the subsurface below the water, so there are P-waves present that were converted from S-waves. The data also contain free-surface multiples.

Aside from the reflection data, a smooth P-wave velocity model is provided and displayed

Table 1: *Recording parameters for the SAGA dataset.*

| Parameter                               | Value          |
|---|----------------|
| Number of source positions              | 399            |
| Source spacing                          | 25 <i>m</i>    |
| First source position                   | 5000 <i>m</i>  |
| Final source position                   | 14950 <i>m</i> |
| Number of receiver positions per source | 180            |
| Receiver spacing                        | 25 <i>m</i>    |
| Minimum receiver offset                 | 150 <i>m</i>   |
| Maximum receiver offset                 | 4625 <i>m</i>  |
| Number of recording samples             | 2001           |
| Sampling interval                       | 0.004 <i>s</i> |
| High-cut Frequency                      | 90 Hz          |

in Figure 3-(b). This model is used to determine the first arrivals required for the Marchenko method. The dashed white box indicates the region of interest that is considered and where the homogeneous Green’s function is retrieved in this paper. Using the reflection data and the velocity model, an image of the region of interest was constructed, which is shown in Figure 3-(c). Imaging is not the main interest of this paper, so the details of the construction are not discussed. More information about imaging using the Marchenko method can be found in Staring et al. (2018). Also note that the retrieval of the homogeneous Green’s function and the construction of the image were done independently of each other. The image will be used to construct a model and to validate the homogeneous Green’s function on the field data. No

induced seismicity recordings are available for this specific area, therefore we cannot use an actual measurement as the source for the homogeneous Green’s function.

Along with the field data, synthetic data were also considered. Because there is no property

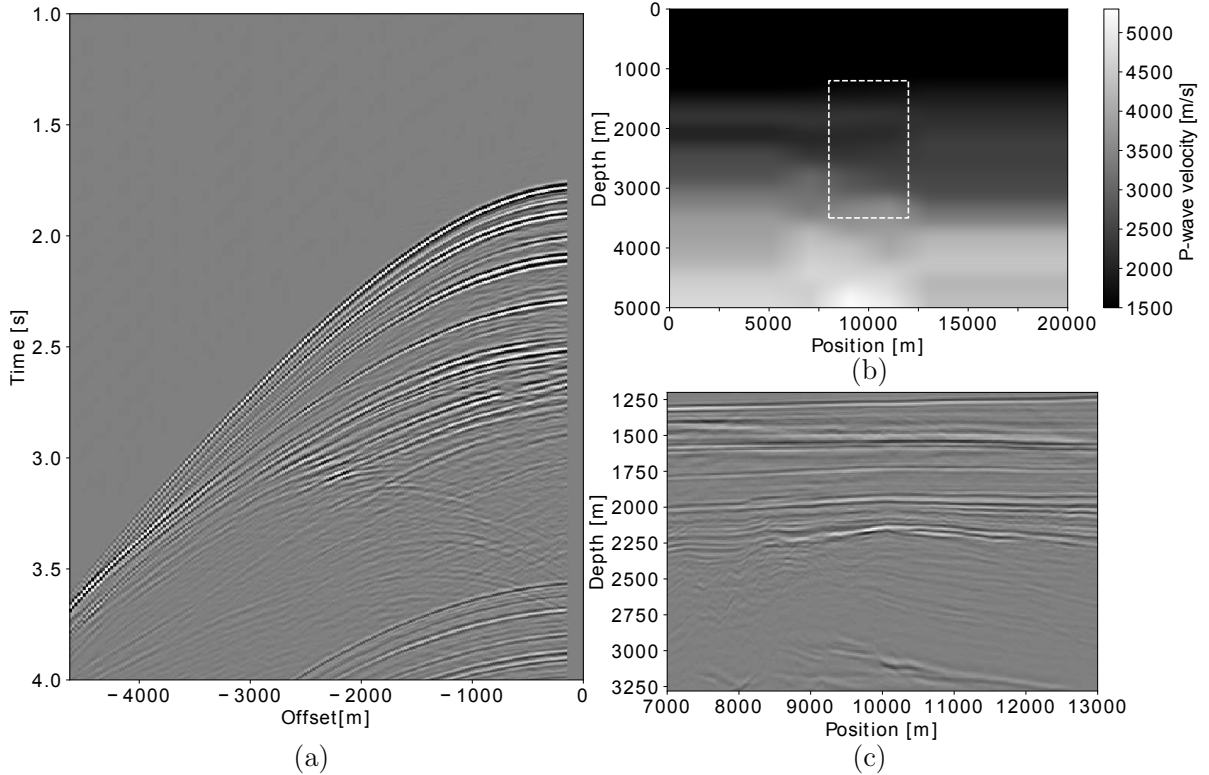


Figure 3: (a) *Unprocessed common-source record of the reflection response recorded over the Vøring basin. The shot is located at zero offset, where along with other near offsets no data could be recorded. Free-surface multiples are present in the data.* (b) *P-wave velocity model in m/s of the area where the data in the Vøring basin were recorded. The white dashed box represents the area of interest.* (c) *Image of the region of interest, indicated by the white dashed box in (b). The data in (a) and (c) have been convolved with a 30 Hz Ricker wavelet for display purposes.*

information of the subsurface available, a model is interpreted based on the image in Figure 3-(c). The image is used to determine the locations of geological contrasts. The velocities are determined by calculating the interval velocities in the smooth velocity model between the contrasts. The interpreted velocity model is displayed in Figure 4-(b), which shows hard boundaries. Notice that below the area of interest the model is homogeneous. It is not possible to achieve reliable imaging in this area, therefore no structures are interpreted. Features outside the region of interest were extrapolated to create a full model. A density model is also constructed in order to ensure strong amplitudes in the reflection data. Because no direct measurements of density in the subsurface are available, the densities are chosen based on realistic ranges. Figure 4-(c) displays the interpreted model. In order to model the synthetic data, the *fdelmodc*-code is used, which was developed by Thorbecke and Draganov (2011). It is a finite-difference modeling code, designed for modeling acoustic and elastic wavefields. There was no S-wave velocity information available and therefore the data as used in this paper are considered to be dominated by acoustic waves. It is possible to use an elastic representation, see Reinicke Urruticoechea and Wapenaar (2017), however for the Vøring basin we do not have the required multi-component data to do so. Using the finite difference method, the reflection response of the interpreted model is computed using the same measurement parameters as

for the real dataset. However, near offsets and positive and negative offsets are included and free-surface multiples are ignored. When comparing Figure 3-(a) and Figure 4-(a), there are similar events, however fewer events are present in the synthetic data. Not all the reflectors in the subsurface can be properly imaged and interpreted, therefore only the major features are present. Because the density information is not available, there is an amplitude mismatch. The converted waves due to elastic interactions from the actual recording are also not taken into account.

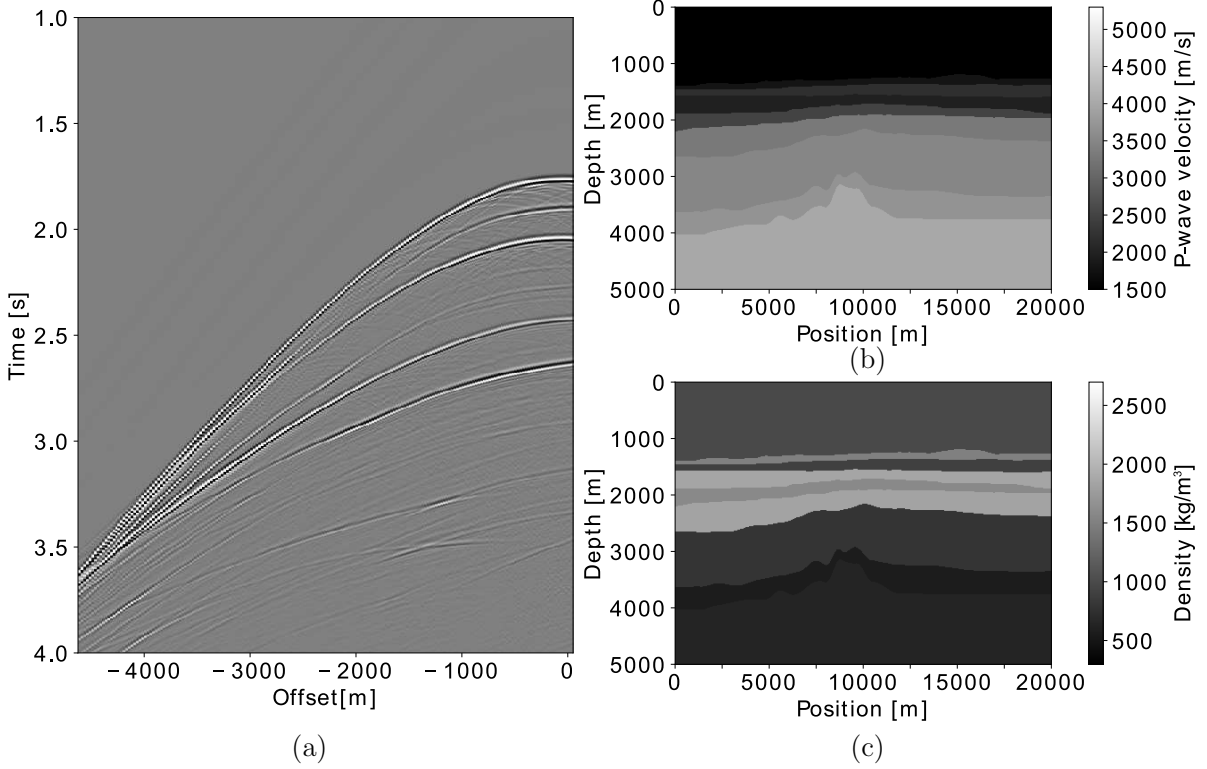


Figure 4: (a) A common-source record of the reflection response modeled using finite-difference modeling in the velocity model from (b) and density model from (c), at the same location as the shot record in Figure 3-(a). The data have been convolved with a 30 Hz Ricker wavelet for display purposes. (b) Synthetic P-wave velocity model in m/s based on the smooth velocity model from Figure 3-(b) and image from Figure 3-(c). (c) Synthetic density model in  $\frac{kg}{m^3}$  based on the image from Figure 3-(c).

### 3.2 Implementation

The raw seismic field reflection data can not directly be used for the Marchenko method, because the method does not converge to a solution. In order to allow the application of the Marchenko method, the field data is preprocessed using different procedures. The general overview of this processing is shown in the flowchart in Figure 5. First of all, source-receiver reciprocity, which states that the source and receiver location of a measurement can be interchanged, is applied. This way a source-receiver pair can also be seen as a receiver-source pair. This allows the offsets in both directions to be constructed. These offsets are vital for the next step, where the "Estimation of Primaries through Sparse Inversion" (EPSI) method is applied. Through the use of the EPSI method, near offsets are reconstructed, the source wavelet is estimated and deconvolved and the free-surface multiples are suppressed. A more detailed consideration of the EPSI method can be found in van Groenestijn and Verschuur (2009). The attenuation on

the data is adaptively corrected for by applying exponential time-gain. The first estimations of this time-gain are based on the velocity model conform the method found in Draganov et al. (2010). Additionally, estimations for the source strength are applied based on the cost functions developed by Brackenhoff (2016). This results in a corrected reflection response that is used by the Marchenko method. The method is tested using these data for a single location. If the method does not converge to a solution, where the artifacts are minimal, the exponential gain and subsequent steps are adjusted and the test is run again. After a few tests we found a solution that did converge with significant removal of artifacts and use this solution for all subsequent runs.

The Marchenko method is applied through the use of software published by Thorbecke et al. (2017). It is an iterative code that takes the reflection response and first arrival data in order to retrieve the focusing functions and Green’s functions. The details of this code are not discussed in this paper, however we do adjust the code in order to apply the corrections for source strength and attenuation required for the reflection response. The first arrivals are modeled using the smooth velocity model shown in Figure 3-(b) and a homogeneous density model. To calculate the first arrival times for the virtual receivers, an eikonal ray tracer is utilized based on the method by Vidale (1988). In order to determine an estimation of the amplitude of the first arrival, we enhance the method using techniques developed by Spetzler and Angelov (2005). For the computation of the first arrival for the synthetic data, the velocity model in Figure 4-(b) is smoothed. For the density model we use a homogeneous density model instead of the model from Figure 4-(c). This is done to replicate the real data situation. The computed first arrival times were also used to determine the required windowing function required in equation (12).

The retrieved Green’s functions and focusing functions are used to evaluate equation (9) and (10). Because there are no induced seismicity recordings to use as source data, we also apply source-receiver reciprocity to one of the virtual receiver locations, to transform it into a virtual source with receiver locations at the surface. The first arrival times for these source positions were not determined using the ray tracer, but rather by modeling them using the *fdelmodc*-code. This is because we consider two source mechanisms, a simple pressure source and a more complex double-couple source. The pressure source is acoustic and is proven to work with the acoustic Marchenko method, while the double-couple source is elastic and produces a response that represents an induced seismicity response, with polarity differences and shifts in the amplitude depending on the angle of the propagating wavefield. To model the response to the double-couple source, we use a homogenous S-wave velocity model of  $1000 \frac{m}{s}$ , except for the top layer where the S-wave velocity is set to zero. This means that no S-waves will arrive at the receiver location. The coda of this modeling will be incorrect, however, as we only use the first arrival, this is of no consequence for our results. The first arrival will be a pure P-wave and contain the characteristics of the double-couple source. The location of the source  $\mathbf{x}_S$  of the Green’s function  $G(\mathbf{x}, \mathbf{x}_S, t)$  is kept constant, which functions as the virtual source position for both the classical and the single-sided approach. The location  $\mathbf{x}_R$  for the receiver of the Green’s function  $G(\mathbf{x}_R, \mathbf{x}, t)$  and the focus for the focusing function  $F(\mathbf{x}_R, \mathbf{x}, t)$  is varied in order to act as a virtual receiver position. In practice, the resulting homogeneous Green’s functions will still contain some artifacts, so in order to remove these, dip filtering is applied. This produces artifacts with low amplitude, which are removed using a time-dependent taper to produce the final estimation of the homogeneous Green’s function.

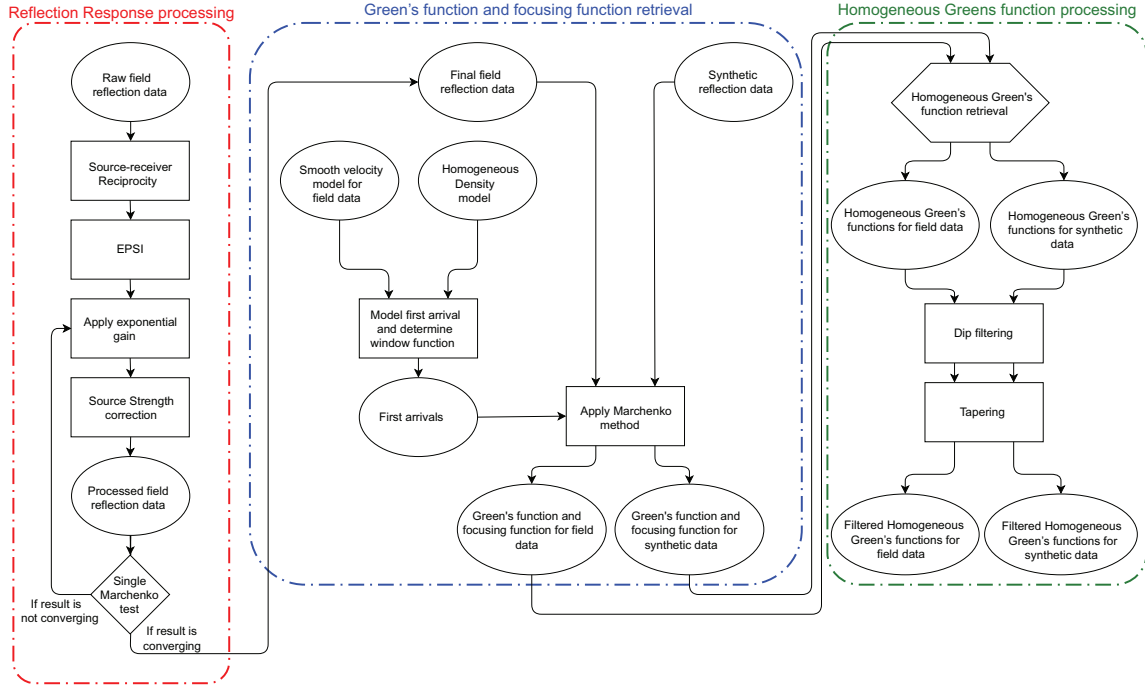


Figure 5: Flowchart for the retrieval of the homogeneous Green's function.

## 4 Results

### 4.1 Retrieval schemes on synthetic data

To demonstrate the advantage of the single-sided representation, we compare different ways of retrieval. We desire to replicate the realistic situation as much as possible, hence the only data that are used are the smooth velocity model from Figure 3-(b) and the modeled reflection response from Figure 4-(a). First, we model the wavefield directly inside the medium by placing the pressure source and receivers inside the region of interest. The wavefield is time-reversed and added to the original wavefield conform equation (4) to create the homogeneous Greens' function. Three snapshots of this result are shown in Figure 6-(a)-(c) at 0 *ms*, 200 *ms* and 400 *ms*. This is the ideal situation, which is used as a benchmark for the other results. The wavefield is convolved with a 15 Hz Ricker wavelet and dotted black lines are shown for reference where scattering should take place. This type of visualization is used for all the snapshots we produce for the synthetic data.

Now, we assume that we do not know the exact model and use the Marchenko method to retrieve Green's functions at many positions in the subsurface. These Green's function are used to evaluate equation (9). The location  $\mathbf{x}_S$  of one response,  $G(\mathbf{x}, \mathbf{x}_S, t)$ , is kept constant as the virtual pressure source position and to serve as a substitute for an induced seismicity recording, while the location  $\mathbf{x}_R$  of the other response  $G(\mathbf{x}_R, \mathbf{x}, t)$ , varies to serve as the virtual receiver position. These positions are exactly the same as the receiver and source positions of the directly modeled wavefield. The retrieved homogeneous Green's function is shown in Figure 6-(d)-(f) at 0 *ms*, 200 *ms* and 400 *ms*. Notice that in this result, compared to the modeled wavefield, the primary upgoing wavefield and the coda of the downgoing wavefield are missing. The downgoing first arrival is present as is the coda of the upgoing wavefield. There are artifacts present throughout the result and particularly at zero time, which in source imaging applications can give doubt over the location of the source. For comparison, we repeat the experiment, however instead of a full Green's function  $G(\mathbf{x}, \mathbf{x}_S, t)$  for the virtual source position, we only use its first arrival to reduce the number of artifacts. The results are shown in Figure 6-(g)-(i) at 0 *ms*, 200 *ms* and 400 *ms*. Compared to the previous experiment, the

number of artifacts decreases, although not all are removed. The strong source artifacts at time zero remain present and the upgoing primary wavefield and downgoing coda are not restored. Using a single arrival does not add any new information, it only removes some of the artifacts. Next we apply the single-sided representation using equation (10). For the virtual source location  $\mathbf{x}_S$  the same response,  $G(\mathbf{x}, \mathbf{x}_S, t)$ , is used as in the previous two experiments. However, the response for the virtual receiver position,  $G(\mathbf{x}_R, \mathbf{x}, t)$ , is replaced by a focusing function,  $F(\mathbf{x}_R, \mathbf{x}, t)$ . Figure 6-(j)-(l) shows the result at 0 *ms*, 200 *ms* and 400 *ms*. The improvement is noticeable, particularly that artifacts are removed. Aside from this, the primary wavefield is reconstructed as is the coda of the downgoing wavefield. When comparing this result to the benchmark, it shows that the events are retrieved at the correct locations and times, although an amplitude mismatch is present. This is due to the fact that the amplitude of the first arrival is not exact, because we assume that we cannot model the first arrival in the real medium. Some of the events are not reconstructed, especially when the angle of the reflection is high. This is because the single-sided boundary is assumed to be infinite, while in reality the aperture is limited. The reflection response lacks certain angles of reflection, so these events cannot be reconstructed. At zero time the snapshot contains less artifacts, however, some remain, which contaminate the result at later times. In order to improve this result, dip filtering is applied to remove these artifacts, as well as a taper. The improved result is shown in Figure 6-(m)-(o) at 0 *ms*, 200 *ms* and 400 *ms*. None of the desired events have been removed, however the artifacts around the source position are gone. When this result is compared to the modeled response, the match is excellent and the improvement over the classical result is significant.

Finally, we consider the same approach, however, we make use of the double-couple source as our source mechanism, instead of the pressure source, to see if the signature has a strong effect on the final result. The first arrival of the double-couple response, where the source is inclined at 20 degrees, is used in the Marchenko method to define a virtual source location. The Green's function for this location is substituted for the one created from a pressure source that was used in the previous examples and the resulting homogeneous Green's function is shown in Figure 6-(p)-(r). The arrival times of the events are the same as the ones retrieved using a pressure source. The main differences are found in the polarity of the events. Due to the double-couple source, the polarity of the wave changes depending on the angle. Because the source we used is inclined, this polarity change is not occurring at 90 and 180 degrees, but rather at 70 and 160 degrees. All events, not just the first arrival, are affected by this, without introducing any additional artifacts. This shows that the double-couple signature can be used in the acoustic scheme that we employ.

## 4.2 Limitations on synthetic data

The reflection response that we use to retrieve the results in Figure 6 is nearly ideal, due to the recording setup and the absence of attenuation. In the following experiment, we perform the homogeneous Green's function retrieval using the single-sided representation and the filtering with five different types of acquisition and data limitations applied to the reflection response. In all five cases we perform the entire process, starting with the Marchenko method to retrieve the focusing function and Green's function from the limited reflection response, followed by applying equation (10) to obtain the homogeneous Green's function for a pressure source. This demonstrates the effects of the limitations of the reflection response on the retrieval scheme. The results of these tests are shown in Figure 7, where (a), (b) and (c), show the result from in Figure 6-(f), (i) and (o), respectively, which are used as a reference. The results shown in the rows below the first one are achieved in the same way as the result from Figure 7-(c), with different types of limitations applied to the reflection response. Each column shows a varying value of the limitation to indicate the sensitivity of the method to these limitations.

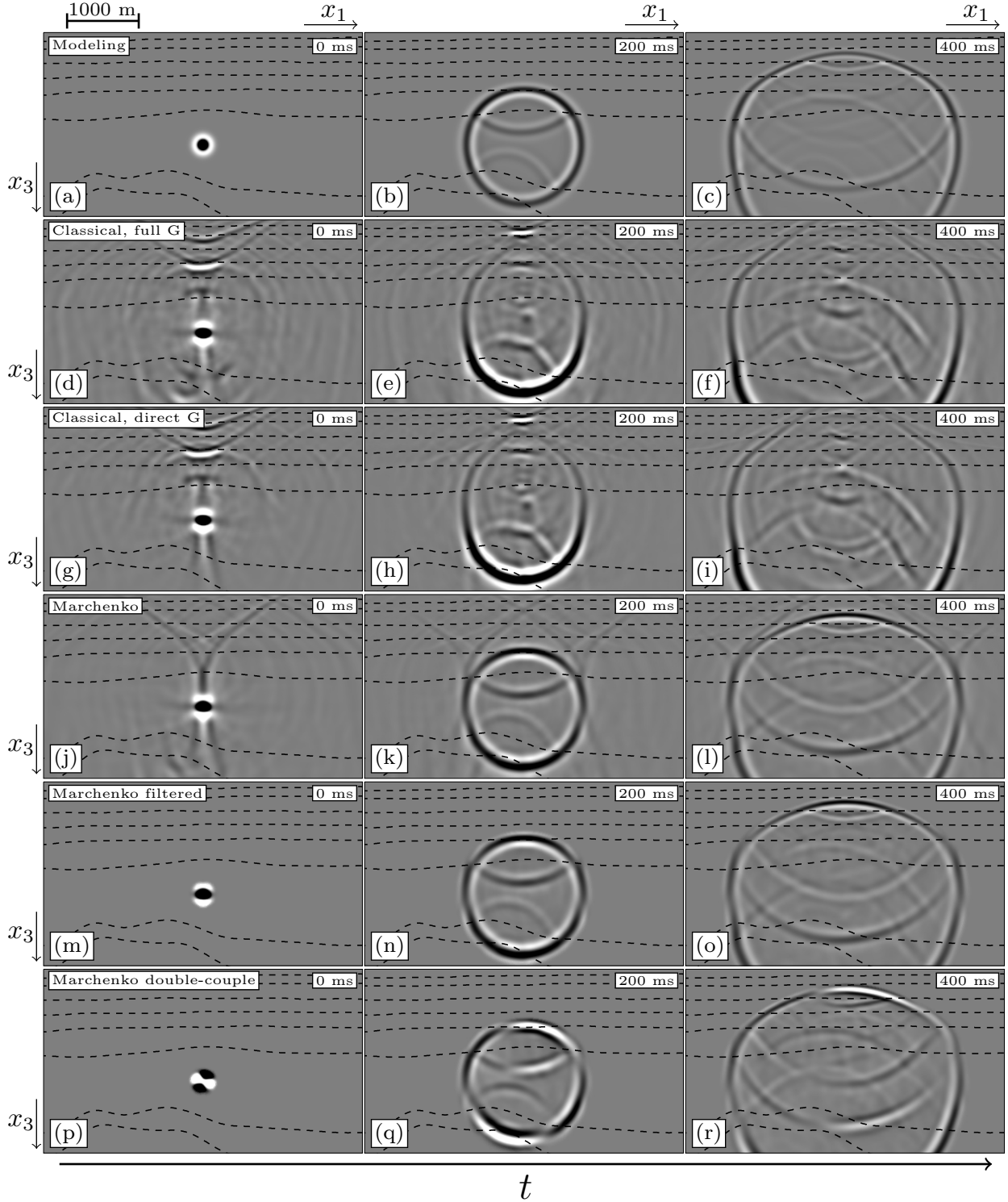


Figure 6: Snapshots of the wavefield at different times. Column 1 indicates  $t=0$  ms, column 2  $t=200$  ms and column 3  $t=400$  ms. All wavefields have been convolved with a 15 Hz Ricker wavelet for display purposes. The black dotted lines indicate the locations of layer interfaces. (a)-(c) Directly modeled homogeneous Green's function in the subsurface used as a reference. (d)-(f) Homogeneous Green's function retrieval using equation (9) with full Green's functions for the virtual source and receiver positions. (g)-(i) Idem, however with a full Green's function for the virtual receiver position and a direct arrival as the Green's function for the virtual source position. (j)-(l) Homogeneous Green's function retrieval using equation (10), a Green's function for the virtual source position and a focusing function for the virtual receiver position, without filtering. (m)-(o) Idem, with dip filtering and tapering applied. (p)-(r) Idem, using a double-couple source inclined at 20 degrees.

In Figure 7-(d)-(f), we display the result retrieved using a reflection response that is sampled coarsely. The sampling values for the receiver and source spacing are 50, 75 and 100  $m$ , which are double, triple and quadruple the original spacing, respectively. Increasing the spacing introduces spatial aliasing that obscures the physical events. When the spacing is doubled, noise is introduced into the final result. The physical events are distorted by this noise and background artifacts are present. This issue is worsened when the spacing distance is tripled. Some events are obscured and strong noise is present. Quadrupling the spacing produces a result that is unusable. It consists almost entirely of noise and the primary events cannot be distinguished. For successful use of the method the events in the reflection response must not be aliased. Hence, the sampling has significant influence on the homogeneous Green's function.

Next, we consider the influence of missing near offsets. The result is shown in Figure 7-(g)-(i), where the first 125, 250 and 500 meters of the offsets are removed from the reflection response, for both positive and negative offsets. When 125 meters of offsets are missing, the result is still comparable to the ideal situation. There is a degradation in quality and few artifacts are present. Removing 250 meters of near offsets increases these issues further, with a stronger degradation of quality. When 500 meters of near offsets are removed, the low angle reflections are not reconstructed properly. The events below and above the virtual source position are missing and strong artifacts are present. These events can be partially removed by adjusting the dip filtering, however, this will also remove the physical events. The near offsets do have an impact on the final result and ideally should be reconstructed, if possible, before applying the Marchenko method.

Figure 7-(j) shows the result using only positive offsets in the reflection response and Figure 7-(k) does the same for negative offsets. In both cases the unwanted artifacts are present and depending on the direction of the offsets, large parts of the events are missing. As mentioned before, when specific angles are not present in the reflection response, they cannot be retrieved in the homogeneous Green's function, so only part of the wavefield is retrieved correctly. Because this issue with the missing direction of the offsets can be easily avoided, by using source-receiver reciprocity, and its effects are strong, it should be taken into account. We perform source-receiver reciprocity on the reflection response containing only the negative offsets and retrieved the result shown in Figure 7-(l). This homogeneous Green's function is similar to the one produced in the ideal situation. We retrieve a similar result when we apply source-receiver reciprocity on the reflection response containing only positive offsets.

The final acquisition limitation that we reviewed was the lack of large offsets, or aperture of the data. In Figure 7-(m)-(o), we show the homogeneous Green's function when the largest offset is, respectively, 2000, 1000 and 500 meters from the source position. When the aperture is 2000 meters, the result is comparable to the ideal situation, with some artifacts introduced. If the aperture is limited to 1000 meters, a result is produced that contains more artifacts and is missing the vertical parts of the desired events. This is once again due to the fact that the angles of this part of the wavefield are not present in the reflection response. If only 500 meters of aperture is available, only the horizontal part of the wavefield is retrieved and the vertical parts are missing. This is clear when Figure 7-(o) is compared to Figure 7-(i). The part of the events that is missing due to the lack of near offsets is present in the case of limited aperture and vice versa. By applying a stronger dip filter, the artifacts can be suppressed, however, as mentioned before, this also removes part of the physical events. Once the data has been recorded, little can be done to increase the aperture, so aperture should be sufficiently large during the actual recording.

Finally, we consider the case of attenuation, which is a factor that cannot directly be influenced during the acquisition of the reflection response. Even if the recording setup is perfect, attenuation of the data is present and can cause a poor result. This is demonstrated in Figure 7-(p)-(r), where the loss applied to the data is  $0.9e^{-0.2t}$ ,  $0.8e^{-0.3t}$  and  $0.7e^{-0.4t}$ , respectively,

in order to simulate the amplitude attenuation on field data. In case of low attenuation, the result still contains the physical events, although they have a lower amplitude. The artifacts are present with a low amplitude. If the attenuation is increased, the physical events start to vanish and the artifacts are more pronounced. In case of high attenuation, the physical events have very low amplitude and there are strong artifacts present.

### 4.3 Field Data

All of the previous limitations are taken into account to apply the Marchenko method, followed by equation (10), on field data. The workflow in Figure 5 is utilized to improve the reflection response for this purpose. After applying source-receiver reciprocity, the EPSI method is used to retrieve the near offsets. We tested interpolation to smaller receiver spacing on the reflection data, however found that it did not significantly improve our results. The reflection response is therefore assumed to have been adequately sampled. To limit the effect of attenuation we test several different time-gains and source strength corrections and find that the Marchenko method operates best when the time-gain is set to  $e^{1.3t}$ , and the source strength correction to 1.73. The only thing we can not improve on is the limited aperture of the data, which will require extrapolation. An example of a common-source record before and after the processing is shown in Figure 8.

After applying all the corrections, The Marchenko method is utilized to retrieve the required Green's functions and focusing functions. These data are retrieved using only a single-sided reflection response and a smooth velocity model. Next, we use the results to retrieve the homogeneous Green's function from the single-sided boundary following equation (10), as shown in Figure 9-(b), (e), (h) and (k), similar to the result in Figure 6-(m)-(o). For comparison, the result of the classical retrieval scheme using only the first arrival for the source Green's function is shown in Figure 9-(a), (d), (g) and (j), similar to the result in Figure 6-(g)-(i). In both cases a pressure source was used for the virtual source. To make a more accurate comparison to using an induced seismicity source, we also use the double-couple source inclined at 20 degrees to create a response for the field data using the Marchenko method. The resulting homogeneous Green's function is shown in Figure 9-(c), (f), (i) and (l). An overlay of the image from Figure 3-(c) is used to indicate locations where scattering is expected. This image is only used for verification. The results of the single-sided representations for the pressure source were previously shown in Wapenaar et al. (2018), but the results for the double-couple source are new.

The snapshots for the single-sided representation for both types of sources show multiple events, upgoing and downgoing. The locations of the scattering and the contrasts on the image overlay have a strong match as well and aside from the primary reflections, the multiple reflections can also be seen. All of these events are completely absent when the classical retrieval is considered. Strong artifacts are present in this case and the coda of the downgoing wavefield is missing entirely. The primary downgoing wavefield is present, however the upgoing primary wavefield is absent, which is similar to the results on the synthetic data. This shows that the single-sided approach is an improvement over the classical approach. There is a difference between the pressure source and the double-couple source, namely the polarity of the events. At the location of the polarity change in the first arrival, there is a decrease in amplitude, which can be seen in the coda as well. This obscures part of the events, which could cause complications when they are to be used for induced seismicity monitoring. This problem appears to be minor and the overall result for the two types of sources are similar and encouraging. However, the method does not produce a perfect result as there are still artifacts present. This is partially due to the presence of background noise in the dataset, which distorts the final result. More coherent events are also present, which do not correlate with the primary wavefield and scattering locations from the image. Because we cannot be sure the reflection

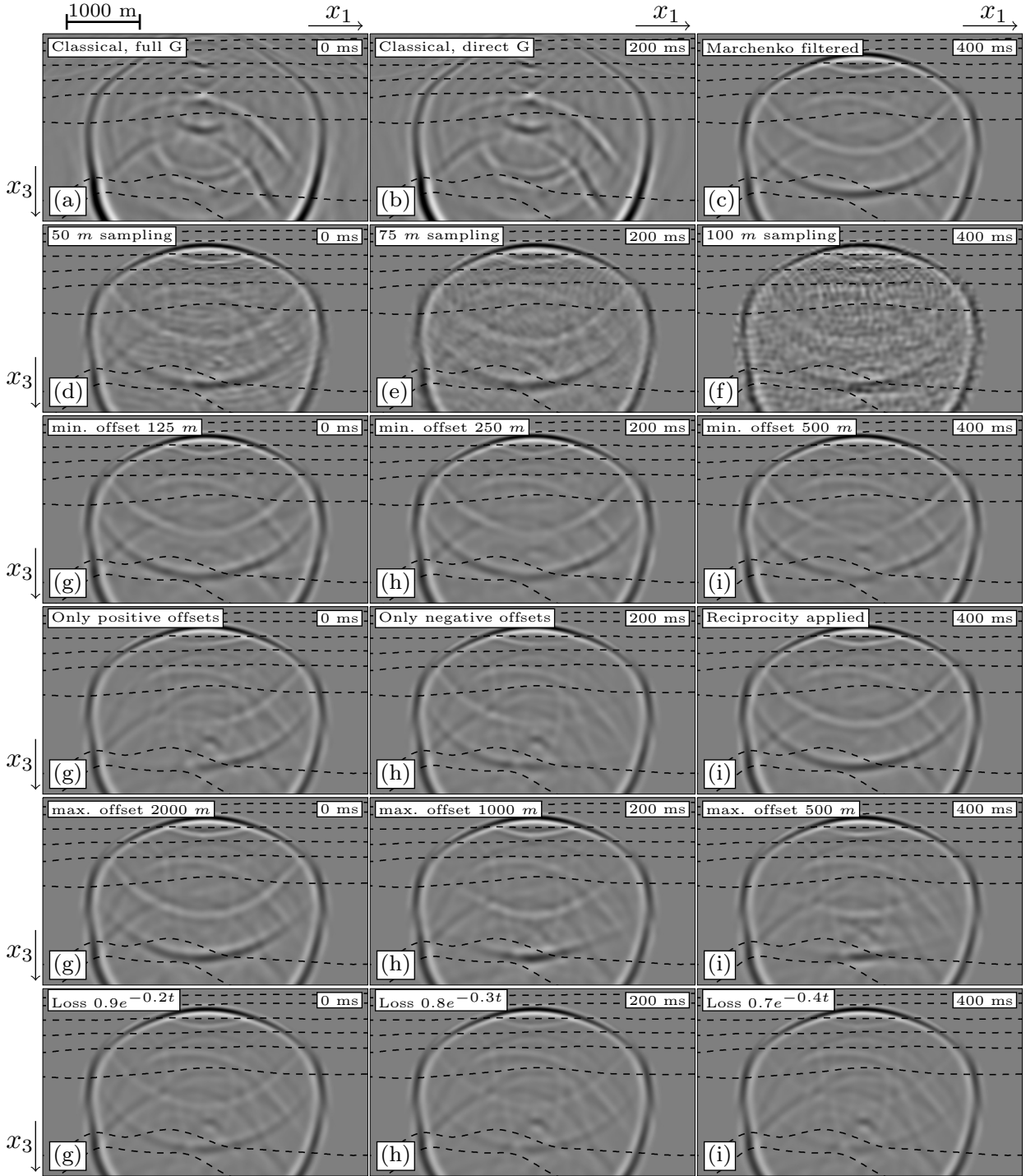


Figure 7: Snapshots of the homogeneous Green's function at  $t=400$  ms retrieved using the Marchenko method and equation (10) and varying limitations of the reflection response. All wavefields have been convolved with a 15 Hz Ricker wavelet for display purposes. (a) The result from Figure 6-(f), (b) the result from Figure 6-(i) and (c) the result from Figure 6-(o), the latter used as a benchmark for the other results. Result when the reflection response has a source and receiver spacing of (d) 50 m, (e) 75 m and (f) 100m. Result when the reflection response is missing the near offsets up to a distance of (g) 125 m, (h) 250 m and (i) 500m. Result when the reflection response contains (j) only positive offsets, (k) only negative offsets and (l) has both offsets restored using source-receiver reciprocity. Result when the reflection response has an aperture limited to (m) 2000 m, (n) 1000 m and (o) 500m. Result when the reflection response has a loss applied to it of (p)  $0.9e^{-0.2t}$ , (q)  $0.8e^{-0.3t}$  and (r)  $0.7e^{-0.4t}$ .

response has been corrected perfectly, there may be some low amplitude artifacts present that are created by the Marchenko method. The Marchenko method that we applied was intended for 2D acoustic media, however, the true medium is 3D and also has elastic properties. As the geological layering appears to be relatively horizontal, the out-of-plane effects are assumed to be low. As mentioned before, the water layer where the sources and receivers are placed is acoustic, however, the actual geological layers are elastic. Due to conversion from P-waves to S-waves and back, some events are present in the reflection response that would not be present if the medium was purely acoustic and are not handled correctly by our acoustic Marchenko implementation.

If we were to use the result from the single-sided representation for our goal of induced seismicity monitoring, we can see that the method produces a very promising result. The source location and mechanism are captured accurately at time zero. The propagation and scattering of the wavefield in the inhomogeneous medium also holds much promise, despite the aforementioned artifacts. If we wanted to track the paths of the wavefronts using this method, a result like this could provide critical insight. When applying this method to actual induced seismicity recordings, there will be additional complications. The source mechanism and location are favorable in the current result, as we could construct these.

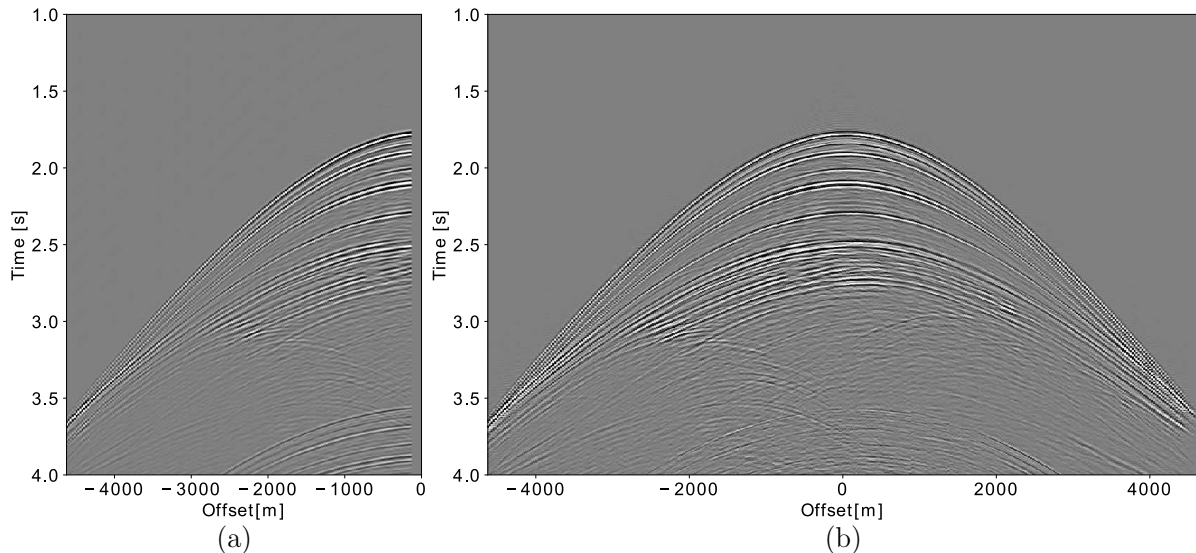


Figure 8: (a) *Common-source record from Figure 3-(a) before any processing is applied and (b) shot record from (a) with source-receiver reciprocity, EPSI and an exponential gain of  $1.73e^{1.3t}$  applied. Both shot records are convolved with a 30 Hz Ricker wavelet for display purposes.*

## 5 Conclusion

We demonstrated the generation of virtual receivers and a virtual source, which have the potential to monitor the subsurface and to predict the complex response of induced seismic sources. We did this by utilizing a single-sided approach to retrieve the homogeneous Green's function in the subsurface. To this end, we applied the Marchenko method, which only requires a single-sided reflection response and a smooth velocity model. We showed that even on synthetic data, with the full Green's function available, the focusing function for the single-sided approach produces better results than the classical approach. The limitations of the Marchenko method were investigated by manipulating the synthetic data. This showed that processing of the reflection response to account for coarse sampling, missing offsets and attenuation is vital for the successful application of the Marchenko method.

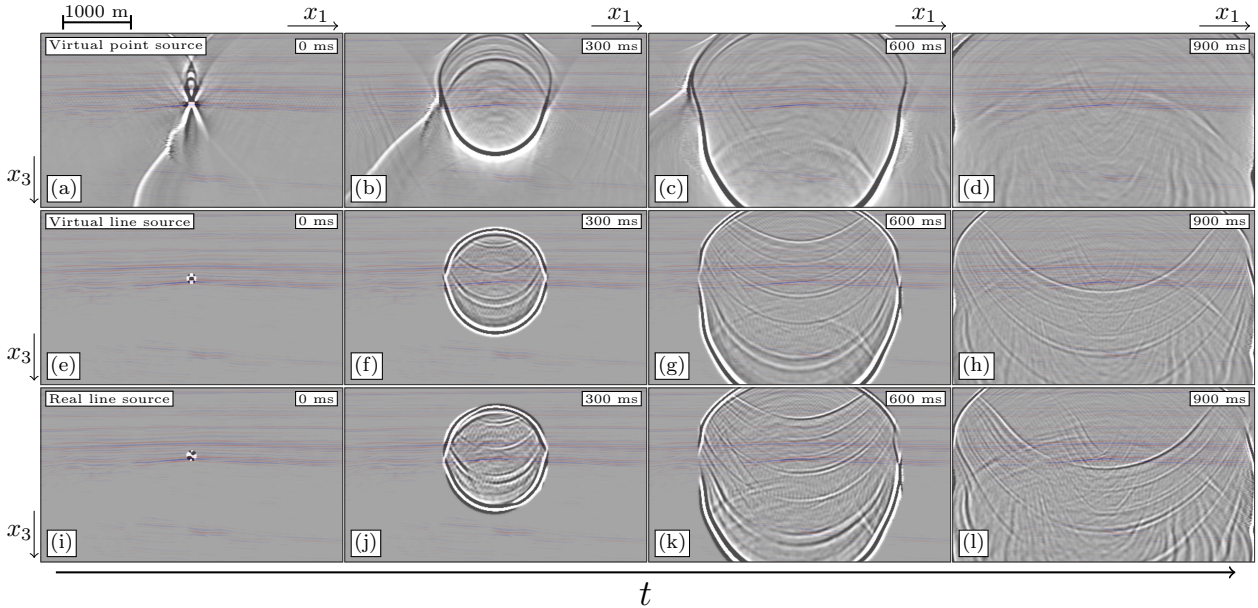


Figure 9: Snapshots of the homogeneous Green's function, convolved with a 30 Hz Ricker wavelet, in the subsurface of the Vøring basin using the classical retrieval scheme for a pressure source from equation (9) at (a) 0 ms, (d) 300 ms, (g) 600 ms and (j) 900 ms. Idem, using the single-sided retrieval scheme for a pressure source from equation (10) at (b) 0 ms, (e) 300 ms, (h) 600 ms and (k) 900 ms. Idem, using the single-sided retrieval scheme for a double-couple source from equation (10) at (c) 0 ms, (f) 300 ms, (i) 600 ms and (l) 900 ms.

We considered a dataset from the Vøring basin, which was affected by these limitations and processed the data using source-receiver reciprocity, the EPSI method and applying a time-gain. The processed reflection response was used to obtain the necessary data to apply the retrieval schemes. The resulting homogeneous Green's function showed potential for wavefield monitoring in the subsurface, as the coda of the wavefield is recovered. The scattering occurs at locations that correlate with an independent image. The pressure source and double-couple source can both be used in the Marchenko method and the resulting homogeneous Green's functions show promise for the goal of induced seismicity monitoring. To further explore this potential, more complex source mechanisms should be considered, such as dynamic fault planes, that are active over an extended area and time period. This includes taking into account the effects caused by elastic media instead of acoustic media.

## Acknowledgements

The authors thank Jan-Willem Vrolijk and Eric Verschuur of the Delphi Consortium for help with processing the data and Equinor for giving permission to use the vintage seismic reflection data of the Vøring Basin. This project has received funding from the European Research Council (ERC) under the European Union's Horizon 2020 research and innovation programme (grant agreement No: 742703). The authors declare no competing interests. The stable versions of the finite-difference modeling code and Marchenko code used in this paper can be found on <https://janth.home.xs4all.nl/Software/OpenSource.tgz>, while the versions in progress can be found on <https://github.com/JanThorbecke/OpenSource>. The seismic reflection data analysed are available from Equinor, but restrictions apply to the availability of these data, which were used under license for the current study, and so are not publicly available. Data are however available from the authors upon reasonable request and with permission of Equinor.

## References

- Brackenhoff, J. (2016). Rescaling of incorrect source strength using Marchenko redatuming. M.sc. thesis, Delft University of Technology, Delft, Zuid-Holland, the Netherlands.
- Broggini, F., Snieder, R., and Wapenaar, K. (2012). Focusing the wavefield inside an unknown 1D medium: Beyond seismic interferometry. *Geophysics*, 77 (5):A25–A28.
- Draganov, D., Ghose, R., Ruigrok, E., Thorbecke, J., and Wapenaar, K. (2010). Seismic interferometry, intrinsic losses and Q-estimation. *Geophysical Prospecting*, 58 (3):361–373.
- Magnani, M. B., Blanpied, M. L., DeShon, H. R., and Hornbach, M. J. (2017). Discriminating between natural versus induced seismicity from long-term deformation history of intraplate faults. *Science advances*, 3(11):e1701593.
- Oristaglio, M. L. (1989). An inverse scattering formula that uses all the data. *Inverse Problems*, 5 (6):1097–1105.
- Porter, R. P. (1970). Diffraction-limited, scalar image formation with holograms of arbitrary shape. *Journal of the Optical Society of America*, 60 (8):1051–1059.
- Porter, R. P. and Devaney, A. J. (1982). Holography and the inverse source problem. *Journal of the Optical Society of America*, 72 (3):327–330.
- Ravasi, M., Vasconcelos, I., Kritski, A., Curtis, A., da Costa Filho, C. A., and Meles, G. A. (2016). Target-oriented Marchenko imaging of a North Sea field. *Geophysical Journal International*, 205 (1):99–104.
- Reinicke Urruticoechea, C. and Wapenaar, K. (2017). Elastodynamic single-sided homogeneous Greens function representation: Theory and examples. In *79th EAGE Conference and Exhibition 2017*, Paris, France. European Association of Geoscientists and Engineers.
- Rose, J. H. (2001). Single-sided focusing of the time-dependent Schrödinger equation. *Physical Review A*, 65 (1):012707.
- Singh, S., Snieder, R., Behura, J., van der Neut, J., Wapenaar, K., and Slob, E. (2015). Marchenko imaging: Imaging with primaries, internal multiples, and free-surface multiples. *Geophysics*, 80 (5):S165–S174.
- Spetzler, J. and Angelov, P. (2005). Ray perturbation theory for traveltime and amplitude attributes in 3D heterogeneous media with weak anisotropy. In *75th SEG Annual Meeting*, Houston, Texas. Society of Exploration Geophysicists.
- Staring, M., Pereira, R., Douma, H., van der Neut, J., and Wapenaar, K. (2018). Source-receiver Marchenko redatuming on field data using an adaptive double-focusing method. *Geophysics*, 83 (6):1–48.
- Thorbecke, J. and Draganov, D. (2011). Finite-difference modeling experiments for seismic interferometry. *Geophysics*, 76 (6):H1–H18.
- Thorbecke, J., Slob, E., Brackenhoff, J., van der Neut, J., and Wapenaar, K. (2017). Implementation of the Marchenko method. *Geophysics*, 82 (6):WB29–WB45.
- van Groenestijn, G. and Verschuur, D. (2009). Estimating primaries by sparse inversion and application to near-offset data reconstruction. *Geophysics*, 74 (3):A23–A28.

- van Thienen-Visser, K. and Breunese, J. (2015). Induced seismicity of the Groningen gas field: History and recent developments. *The Leading Edge*, 34 (6):664–671.
- Vidale, J. (1988). Finite-difference calculation of travel times. *Bulletin of the Seismological Society of America*, 78 (6):2062–2076.
- Wapenaar, K., Brackenhoff, J., Thorbecke, J., van der Neut, J., Slob, E., and Verschuur, E. (2018). Virtual acoustics in inhomogeneous media with single-sided access. *Scientific Reports*, 8 (1):2497.
- Wapenaar, K., Thorbecke, J., and van der Neut, J. (2016). A single-sided homogeneous Green’s function representation for holographic imaging, inverse scattering, time-reversal acoustics and interferometric Green’s function retrieval. *Geophysical Journal International*, 205 (1):531–535.
- Wapenaar, K., Thorbecke, J., van Der Neut, J., Brogini, F., Slob, E., and Snieder, R. (2014). Marchenko imaging. *Geophysics*, 79 (3):WA39–WA57.
- Wapenaar, K., Thorbecke, J., van der Neut, J., Slob, E., and Snieder, R. (2017). Virtual sources and their responses, Part II: data-driven single-sided focusing. *Geophysical Prospecting*, 65 (6):1430–1451.